

Structural and Fracture Mechanics Study of a Pipe with a Circumferential Crack under Blowdown-Induced Loading

S. BROSI, R. WANNER, K. REICHLIN
Paul Scherrer Institute, Würenlingen, Switzerland

D. SCHRAMMEL
Kernforschungszentrum Karlsruhe, Karlsruhe, FRG

E. KOBES
University of Stuttgart, Stuttgart, FRG

1 INTRODUCTION

The test series E31 of the German HDR Safety Program investigates the transferability of 'leak before break' data obtained in laboratory tests to a real piping. Within this test series the fullscale blowdown experiment E31.2 (Schrammel et al. 1990; Kussmaul et al. 1991) was performed with a test configuration similar to a boiling water reactor feedwater piping, connected to a pressure vessel. This 25 m long piping of complex shape, with an inner diameter of 425 mm, contained a circumferential, internal surface crack of an initial arc length $2\alpha = 60^\circ$ and an initial depth relative to the wall thickness $a/w = 0.3$. A blowdown was initiated by a simulated pipe break at temperature $T = 240^\circ\text{C}$ and internal pressure $p = 9\text{ MPa}$. The pressure drop and a waterhammer, induced by a rapid closure of a feedwater check valve, caused pipe oscillations which effected a high bending load in the crack area and therefore large axial stresses and strains respectively. The bending stress attained its peak value at 30° from the crack symmetry line. A maximum stable crack growth of 1.5 mm and large plastic deformations in the crack region resulted.

The present numerical study has two objectives. The first one is to establish the overall reaction of the piping and the second one is to analyse the stress in the crack zone. The calculations presented here are first steps in an ongoing comprehensive piping analysis which is performed by several institutes. In these first steps several simplifications are made, such as linear elastic material behavior. The experience gained in the linear analysis will allow one to adapt the calculation models for the nonlinear analysis to the fairly well known piping reaction. The linear crack analysis provides a qualitative insight into the time variation of the stress intensity along the crack front due to the large variation of the bending axis direction that has been observed in the experiment; furthermore, it allows a check of the finite element (FE) model by comparison of its results with existing solutions.

2 PIPING ANALYSIS

2.1 Calculation Model

The structural dynamics study of the total piping was performed with the FE program ADINA. In order to establish an adequate calculation model, extensive parameter studies with variation of element type, integration order, mesh refinement, time increment, Rayleigh damping factors, etc. were performed. The calculation model finally chosen is described below and shown in detail in Fig. 1. Due to the assumption of linear elastic material behavior the influence of the small surface flaw on the piping flexibility could be considered to be very small and therefore was neglected. The unflawed piping was discretized with 59 4-node pipe elements, each of straight or curved shape and constant cross section. Each element node had three displacement degrees of freedom (d.o.f.), three rotational d.o.f. and six ovalization d.o.f.. Due to the assumed linearity, only small displacements and small strains were considered. Newton-Cotes integration was used for the element stiffness generation; Newmark direct time integration and Rayleigh damping were applied in the analysis. The pipe end connected to the reactor pressure vessel (RPV) was rigidly fixed, whereas the other pipe end was slightly flexible. At that end the relation between the pipe deflection (displacement \vec{u} , rotation $\vec{\phi}$) and the support reaction (force \vec{F} , moment \vec{M}) is given by the stiffness matrix shown in Fig. 1. The dynamic loading was applied by the elbow forces $\vec{F}_e(t)$ which were calculated from the pipe internal pressure time history recorded in the experiment. With $p_e(t)$ equal to the pressure at the center e

SMiRT 11 Transactions Vol. F (August 1991) Tokyo, Japan, © 1991

of the elbow at time t , the absolute value of the elbow force is given by $|\vec{F}_e|(t) = \pi r_e^2 p_e(t)$. The global piping calculation ran with a time increment of 1 ms from 5 ms after blowdown initiation up to 298 ms and took one hour CPU time on a CRAY-2 computer.

2.2 Results

In order to assess the correspondence between experiment and calculation for a variable vector parameter one has separately to consider its absolute value and its direction for any given time. For the dynamic part of the calculated and measured radial displacement $\vec{u}_r = (u_y, u_z)$ of the center of the pipe cross section Q46 Fig. 2 shows the time history of $|\vec{u}_r|$ for the full time interval considered and Fig. 3 shows the locus of \vec{u}_r for the reduced time interval up to 150 ms. It can be seen that the center of Q46 moves on a clockwise oriented curve in the yz -plane, i.e. perpendicular to the pipe axis, first up ($A \rightarrow B$) and then down to its maximum deflection at D. The time t_D of highest $|\vec{u}_r|$ value agrees very well between experiment ($t_D = 109$ ms) and calculation ($t_D = 110$ ms). The results of the linear calculation should be compared with the experimental ones up to t_D only, since in the experiment at approximately this time large plastic deformations occurred in the weakened pipe region of the test piece. For the time interval considered it can be concluded from Fig. 2 and 3 that qualitatively \vec{u}_r agrees well between experiment and calculation. Quantitatively the calculated displacements differ from the measured ones considerably more than expected. Especially the large discrepancy at the beginning ($A \rightarrow C$), i.e. at times when no plastification has yet occurred, is surprising. At t_B , the time of the first radial displacement relative maximum, the calculated displacement $|\vec{u}_r|$ is 28 % lower than the measured one. This discrepancy is reduced to 18 % at time t_D . From Fig. 3 it can be seen that the calculated displacement component in z -direction deviates proportionally less than the one in y -direction. This finding is not fully understood yet and will have to be studied in detail. For the time t_D the calculated deformation of the whole piping is shown in Fig. 4. Basically one can recognize two global deflections: a translation in negative z -direction and a clockwise rotation around the x -axis.

In the following, the dynamic part of the calculated bending moment is discussed and compared with the experimental one which was determined from strains monitored by the strain gages located next to the plastic zone. The time history and the locus of the resultant bending moment $\vec{M}_b = (M_y, M_z)$ in the pipe cross section QP1 are plotted in Fig. 5 and 6. The moment \vec{M}_b in QP1 basically corresponds to the already discussed displacement \vec{u}_r in Q46. Good agreement between calculation and experiment can be noticed up to time $t_P \approx 93$ ms; the small deviation occurs due to a high frequency oscillation which is superimposed to the basic pipe oscillation and which in the experiment is excited more strongly. After t_P the influence of the high plastification can clearly be seen, in the experiment QP1 is not able to carry a higher bending moment anymore. The calculated values of $|\vec{M}_b|$ for $t = 106$ ms and the upper limit for the time interval $t = 0$ ms \sim 300 ms are plotted in Fig. 7 versus the pipe axis path s with its origin at the RPV, equal to the origin of the global coordinate system (x, y, z) . It turns out that the highest bending moment observed throughout the whole calculation appears at time $t = 106$ ms at the pipe end connected to the RPV and that therefore QP1 with its considerably reduced wall thickness is the most highly stressed cross section of the whole piping. Furthermore it can be seen that at time of maximum stress in QP1 ($t = 106$ ms) most pipe cross sections experience a high stress level relative to the highest one calculated for each.

For QP1 the calculated time history of σ_I , the effective stress according to the German design rule KTA 3201.2, equation 3.5-1, is plotted in Fig. 8. It can be seen that its maximum value is 60 % higher than the maximum allowable KTA value $3 S_m$. Since the piping did not lose integrity in the test, it is clearly shown that even for the considered degraded piping the design rule is conservative.

3 CRACK ANALYSIS

3.1 Calculation Model

For the FE analysis a straight pipe with an internal circumferential surface crack, inner diameter $d_i = 425$ mm, wall thickness $w = 16$ mm and length $l = 1000$ mm was discretized with 1836 20-node brick elements and 7470 nodes (Fig. 9); each node had three displacement d.o.f.. The crack plane according to QP1 of the test piece (Fig. 1) is the models one pipe end, here assumed to be a symmetry plane. As in the experiment, the crack is positioned in the upper half of the cross section and symmetric with respect to the z -axis. Both the measured and the modelled crack shape are shown in Fig. 10. The crack front is modelled by an eccentric arc, completed by a quarter of an ellipse at each end. The crack tip zone is modelled by six circumferential wedge elements with a $1/\sqrt{r}$ singularity. Since in the experiment the crack cross section essentially experienced bending load, pure bending was assumed for the calculation and applied at the other pipe end with 3D pressure loading equivalent to the bending stresses. The stress intensity factor K_I was computed from the energy release rate G by the relationship for plain strain

condition, using the virtual crack extension scheme shown in Fig. 9. G as calculated by ADINA divided by the perturbed area and G as computed by the fracture mechanics post processor ORVIRT based on an ADINA stress analysis were found to be identical. The stress analysis took 1000 CPU seconds on a CRAY-2 computer.

3.2 Results

Fig. 11 shows the specific K_I factor for $|\vec{M}_b| = 1 \text{ MNm}$ and for the bending orientation angle $\gamma = 0^\circ \sim 90^\circ$ versus the crack front position φ . K_I was computed for $\gamma = 0^\circ$ and 90° only; for other values of γ it was obtained by superposition. $K_{I,U}$ was found to be 12% smaller than the handbook solution for a semielliptical crack with the same maximum depth (Murakami et al. 1987) which is based on line spring elements and for which a maximum deviation of 10 % from an exact solution is postulated. For axial cracks it was shown that the handbook solution overestimates K_I , but the discrepancy in our case is larger. With the dashed line in Fig. 11 it is shown that for increasing values of γ the value $K_{I,max}$ of the maximum stress intensity along the crack front decreases whereas $\varphi(K_{I,max})$ increases. Note that for $\gamma = 30^\circ$, measured in QP1 for the maximum $|\vec{M}_b|$ at $t = 104 \text{ ms}$, the left crack side ($\varphi > 0^\circ$) is partially slightly more loaded, the right crack side is substantially less loaded and $K_{I,max}$ is 10 % smaller, compared to the case of $\gamma = 0^\circ$.

$K_{I,max}$ and $K_I(\varphi = 0^\circ)$ for the load history of the experiment, obtained by superposition from the specific K_I factors, are plotted in Fig. 12 for two different circumferential crack positions. The lower two curves correspond to the crack position of the experiment. The upper two curves are related to a crack position rotated by 30° relative to the experimental one. For the rotated position the maximum bending stress appears at the crack center and therefore, as can be seen from Fig 11, one can thus find the upper limit of K_I which can be reached for any given crack position. The values for $K_{I,U}$, $K_{I,V}$ and $K_{I,W}$ are plotted in Fig. 12; their position φ is shown in Fig. 11.

4 CONCLUSIONS

For an unflawed piping the linear global structural dynamic response after pipe break and undamped closure of a check valve was studied; furthermore with a local pipe model containing a circumferential internal surface crack the influence of bending direction on the stress intensity was investigated for both a uniform bending moment and for the loading as measured in the experiment.

Up to ca. 93 ms the bending moments of calculation and experiment agree very well; the agreement for the pipe deflection however is good in quality only. Quantitatively the discrepancy between measured and calculated displacements is surprisingly large. After 93 ms better results can be expected from a calculation with a nonlinear material law which is able to include the high level of plastification occurred in the experiment. But before performing this expensive calculation, the reason for the mentioned displacement discrepancy should be found. From the comparison of the calculated effective stress with the design limit $3 S_m$ it could be shown that the KTA design rule is conservative even for the considered flawed piping. Due to asymmetrical loading one crack half is substantially less stressed than the other one. The maximum K_I for a crack of the same shape as the measured one but at any different circumferential position is 10% higher than $K_{I,max}$ for the experimental position.

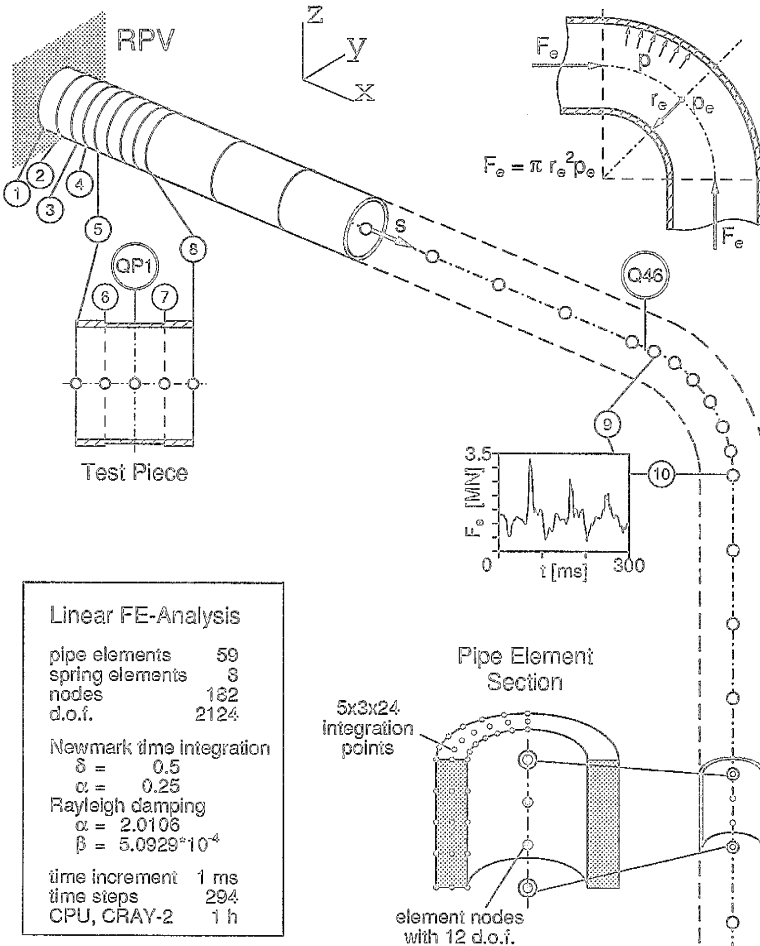
ACKNOWLEDGEMENTS

We wish to express our gratitude to Dr. R. Rösel and G. Duijvestijn from the Paul Scherrer Institute for their support to the present work. We gratefully mention the financial assistance from the Swiss Federal Nuclear Safety Inspectorate and from the Swiss Federal Office of Energy.

REFERENCES

- Kussmaul, K., Diem, H., Kobes, E., Brosi, S., and Schrammel, D. (1991): Load Bearing Capacity of a Degraded Pipe System When Subjected to a Blowdown-induced Waterhammer. Transactions of the 11th SMIRT Conference, Tokyo.
- Murakami et al. (1987): Stress Intensity Factors Handbook. Committee on Fracture Mechanics, The Society of Material Science, Japan, Vol. 2, pp 759-770.
- Schrammel, D. and Brosi, S. (1990): Auslegungsbericht zu Versuchsgruppe E31 (BLORI), PHDR-Arbeitsbericht Nr. 30.018/90.

Fig. 1: Global piping FE model.



Pipe Geometry [mm]

Pipe Axis Coordinates

	x	y	z
1:	142	0	0
QP1:	856	0	0
Q46:	5300	0	0
9:	5348	0	0
10:	6041	0	-693
11:	6041	0	-8070
12:	6041	-1000	-7070
13:	6041	-1949	-7070
14:	6041	-2949	-6070
15:	6041	-2949	-5970
16:	5175	-3449	-4970
17:	2739	-4856	-4970

Segment Dimensions

	\$d_i\$	\$w\$	\$l\$
1-2:	439	111	157
2-3:	446	70	128
3-4:	445	33	102
4-5:	424	26	102
5-6:	425	25	110
6-7:	425	16	230
7-9:	425	25	4377
9-10:	429	30	1088
10-17:	425	25	13949

Elbow Radii

9-10:	693
11-12:	1000
13-14:	1000
15-16:	1000

Linear FE-Analysis

pipe elements	59
spring elements	6
nodes	162
d.o.f.	2124

Newmark time integration

\$\delta = 0.5\$

\$\alpha = 0.25\$

Rayleigh damping

\$\alpha = 2.0106\$

\$\beta = 5.0929 \cdot 10^{-4}\$

time increment 1 ms

time steps 294

CPU, CRAY-2 1 h

Material Properties, T = 240 °C

Young's modulus: \$E = 196\ 000\$ MPa

Poisson's ratio: \$\nu = 0.3\$

density: \$\rho = 11\ 530\$ Kg/m³

Support Stiffness

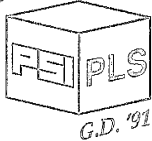
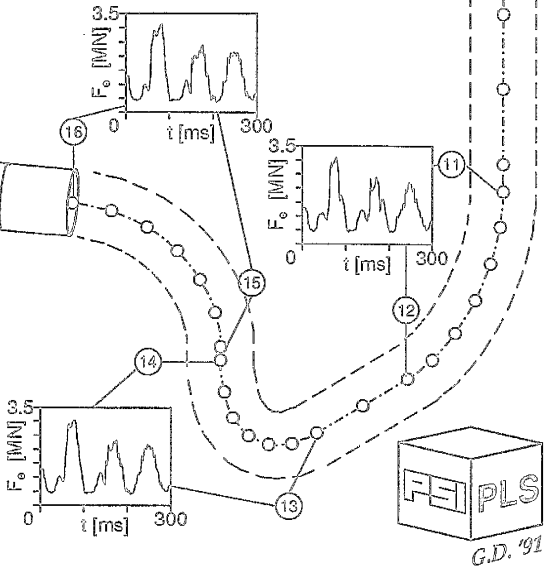
$$\begin{bmatrix} F_x \\ F_y \\ F_z \\ M_x \\ M_y \\ M_z \end{bmatrix} = \begin{bmatrix} k_{11} & k_{12} & 0 & 0 & 0 & 0 \\ & k_{22} & 0 & 0 & 0 & 0 \\ & & k_{33} & 0 & 0 & 0 \\ & & & k_{44} & k_{45} & 0 \\ & & & & k_{55} & 0 \\ & & & & & k_{66} \end{bmatrix} \begin{bmatrix} u_x \\ u_y \\ u_z \\ \phi_x \\ \phi_y \\ \phi_z \end{bmatrix}$$

\$k_{11} = 2.0628\$ GN/m \$k_{44} = 1.2692\$ GNm/rad

\$k_{12} = 0.8613\$ GN/m \$k_{45} = 0.4690\$ GNm/rad

\$k_{22} = 1.0683\$ GN/m \$k_{55} = 0.7278\$ GNm/rad

\$k_{33} = 8.7700\$ GN/m \$k_{66} = 0.6370\$ GNm/rad



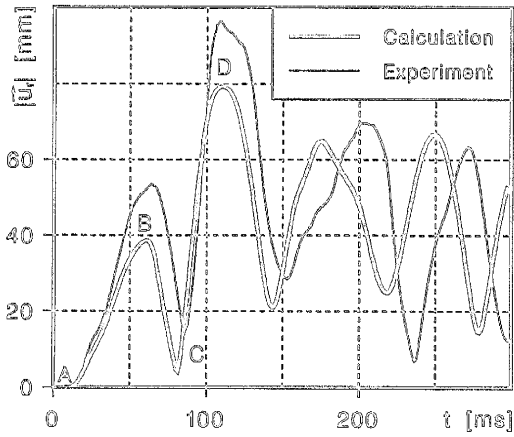


Fig. 2: Radial displacement $|\bar{u}_r|$ in Q46.

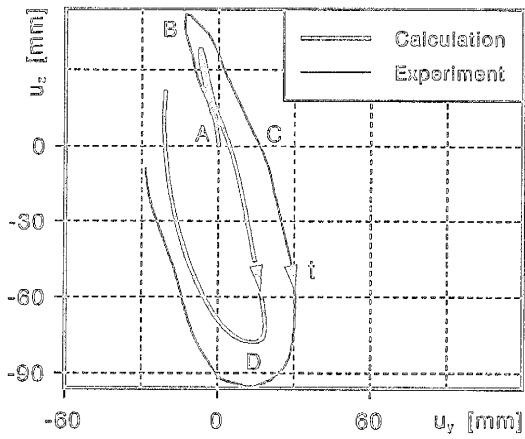


Fig. 3: Locus of \bar{u}_r in Q46, $t = 0 \text{ ms} \sim 150 \text{ ms}$.

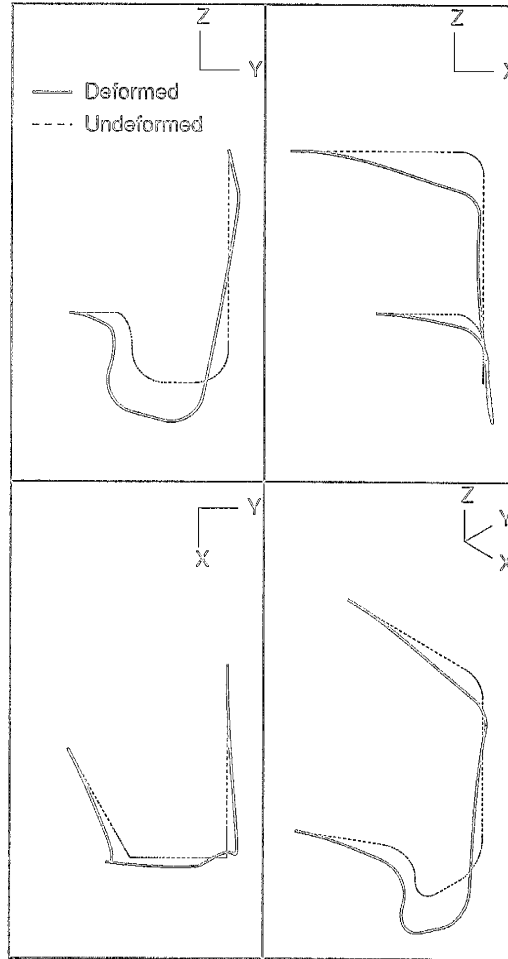


Fig. 4: Amplified pipe deflection at time t_D .

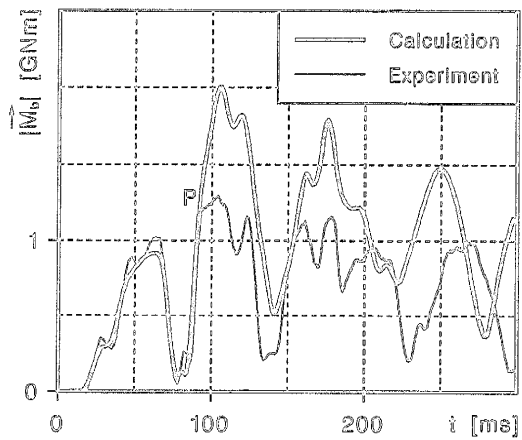


Fig. 5: Resultant bending moment $|\bar{M}_b|$ in QP1.

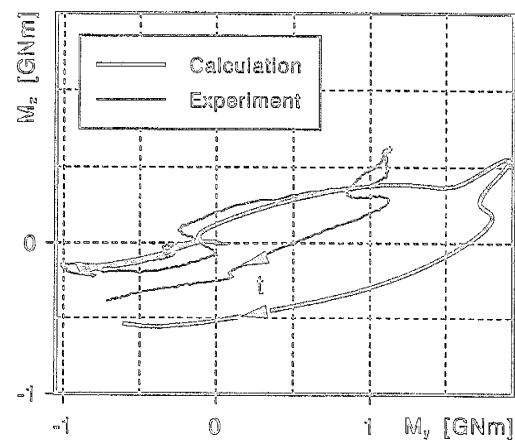


Fig. 6: Locus of \bar{M}_b in QP1, $t = 0 \text{ ms} \sim 150 \text{ ms}$.

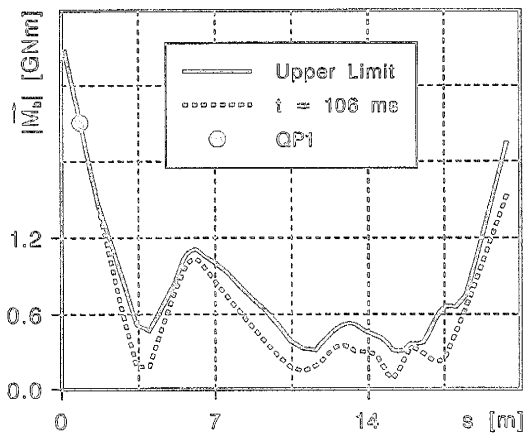


Fig. 7: Bending moment $|\vec{M}_b|$ along the piping.

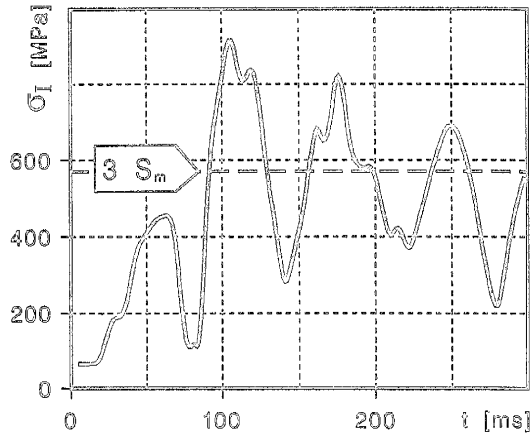


Fig. 8: KTA effective stress σ_I in QP1.

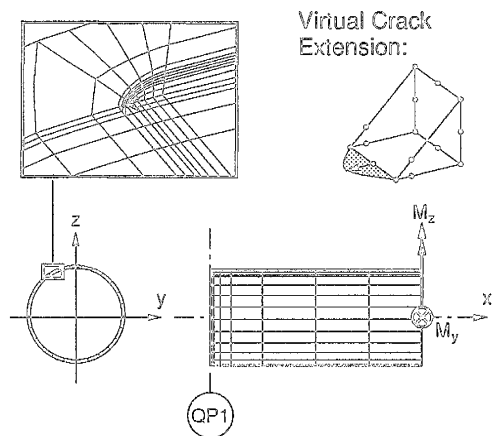


Fig. 9: Crack analysis FE model with 21993 d.o.f.

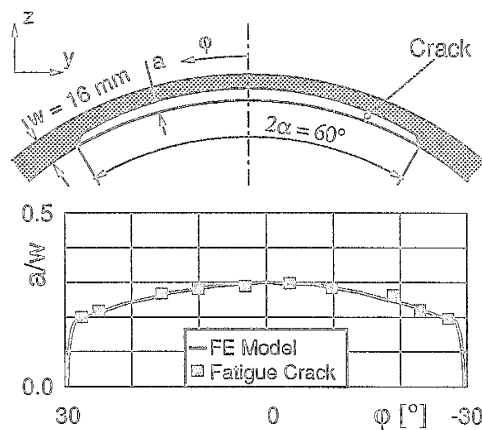


Fig. 10: Modelled and measured crack geometry.

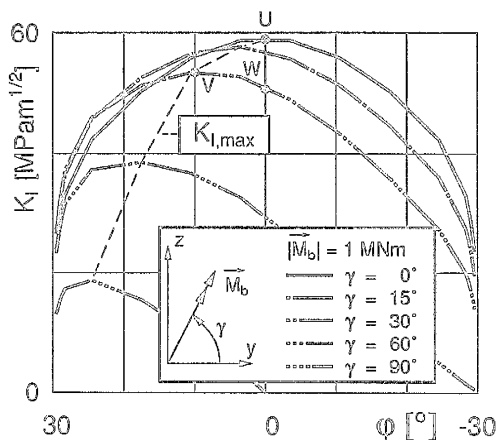


Fig. 11: Specific K_I factor for $|\vec{M}_b| = 1 \text{ MNm}$.

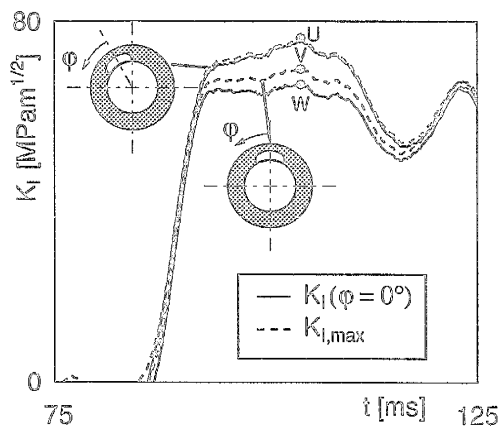


Fig. 12: K_I for the blowdown loading.